

# Numerical Simulations of Phase Transitions in Crystals and a Global Free Energy Minimisation Algorithm

T. Blesgen<sup>1,†</sup> and U. Weikard<sup>2</sup>

<sup>1</sup> *Max-Planck-Institute for Mathematics in the Sciences,  
Inselstraße 22-26, 04103 Leipzig, Germany,*

*EMail: blesgen@mis.mpg.de, Phone:+49(341) 9959-804*

<sup>†</sup> *Corresponding author*

<sup>2</sup> *Faculty of Mathematics, University of Duisburg-Essen,  
Lotharstraße 65, 47048 Duisburg, Germany,*

*EMail: wk@math.uni-duisburg.de, Phone:+49(203)379 4049*

## **Abstract:**

A model describing phase transitions in crystals coupled with diffusion and linear elasticity under isothermal conditions is studied numerically in two space dimensions. For the minimisation of the free energy w.r.t. the phase parameter an algorithm based on the level set approach is presented together with an extension based on the isoperimetric inequality that allows to find a global minimum in most cases.

# 1 Introduction

The model we are going to study here was introduced in [4] and explains phase transitions for a certain class of materials that is characterised below. The equations are related to the Stefan model but allow for deformation and there is no diffusion of latent heat inherent in the new model. A survey of results on the Stefan problem can for instance be found in [6] and [8].

Generically, we will restrict in this article to the case of at most two co-existing phases and assume that a linear stress-strain relationship holds. A formulation that accounts for non-linear stress-strain laws is in preparation, [1], but the techniques of this existence proof are fully non-linear and differ considerably from [4], as suitable growth conditions have to be imposed on the gradient of the deformation that exclude the case of linear elasticity treated here.

We will focus on the numerical analysis of the model which is the content of Sections 3, 4 and 6. A main aspect of the mathematical formulation is that the phase parameter is the *global* minimiser of the free energy. In many physical applications this assumption is not reasonable, as a global minimum is not achieved or only after a very long time. Yet, for so-called diffusion induced segregation (DIS) processes the segregation into two phases only starts after the concentration of a diffusor exceeds a certain threshold. As the diffusor dramatically changes the local lattice order of the crystal, there is a high start energy and it is reasonable to assume that (at least approximately) a global minimiser of the free energy is reached in short time, see [3] for details. The crystallography of DIS-phenomena is discussed in [2].

For the numerical scheme the computation of a global minimiser represents a real challenge. To overcome the difficulties, in Section 4 we first develop a basic algorithm, then an extension. The basic algorithm uses a front propagation similar to the fast marching method, the extension exploits the isoperimetric inequality. This inequality supplies us with a sufficient criterium when no interface can be present. As we shall demonstrate, the extended algorithm finds in most cases a solution close to the global optimum with a systematic error of the order  $O(h)$  where  $h$  is the maximal distance of two neighbouring vertices of the triangulation.

In Section 5 we shortly compute a radially symmetric stationary solution used to test the code. We finish with the presentation of some numerical results that illustrate the behaviour of the algorithm.

## 2 Summary of the model

The complete derivation of the model can be found in [4], where also the existence of global solutions is proved. For convenience we repeat here the equations and restate the main existence result.

Let  $\Omega \subset \mathbb{R}^D$ ,  $1 \leq D \leq 3$  be a bounded domain with Lipschitz boundary that represents the crystal. By  $H^{m,2}(\Omega)$  we denote the Sobolev space of  $m$ -times weakly differentiable functions in the Hilbert space  $L^2(\Omega)$ , by  $H_0^{m,2}(\Omega)$  the closure of  $C_0^\infty(\Omega)$  w.r.t.  $\|\cdot\|_{H^{1,2}(\Omega)}$  and by  $BV(\Omega)$  the space of functions with bounded variation, see for instance [9].  $C_0^\infty(\Omega) := \cap_{m=0}^\infty C_0^m(\Omega)$  where  $C_0^m(\Omega)$  is the space of  $m$ -times continuously differentiable functions over  $\Omega$  with compact support.

The particle densities of the  $n$  different species of molecules are determined by  $\varrho_i = \varrho_i(x, t)$ . Let  $\varrho := (\varrho_1, \dots, \varrho_n)$  be the density vector where  $\varrho_i \geq 0$ ,  $\varrho_i \in H^{1,2}(\Omega)$  and, due to the possible presense of vacancies,  $\sum_{i=1}^n \varrho_i \leq 1$ .

For the diffusive flux  $J$  we assume Onsager's law  $J(t) = L\nabla\mu(t)$  where  $\nabla\mu := (\nabla\mu_1, \dots, \nabla\mu_n)$  is the vector of chemical potentials and  $L$  the (constant)  $n \times n$  mobility tensor.

We introduce a phase function  $\chi = \chi(\cdot, t) \in X$ ,  $X := BV(\Omega, \{0, 1\})$ , that is the characteristic function of one a priori chosen phase. As the range of  $\chi$  is finite, we obtain a sharp interface model. For later use we make the appointment  $\chi_1 := \chi$ ,  $\chi_2 := 1 - \chi$ .

For deformation vectors  $u = (u_1, \dots, u_D)$  let  $f_j = f_j(\varrho, u)$  be the free energy density of phase  $j$ ,  $j = 1, 2$ .  $f_j$  are smooth functions; standard examples are the in  $\varrho$  convex functionals

$$f_j(\varrho, u) := \sum_{i=1}^n \frac{\hat{\varrho}_{ij}}{2} (\varrho_i - \bar{\varrho}_{ij})^2 + W_j^{el}(u), \quad (1)$$

$$f_j(\varrho, u) := \alpha_j \sum_{i=1}^n \varrho_i \ln \varrho_i + W_j^{el}(u). \quad (2)$$

In (1), (2),  $\hat{\varrho}_{ij}$  and  $\alpha_j$  are positive constants and the elastic energy is

$$W_j^{el}(u) := \frac{1}{2} (\mathcal{E}(u) - \bar{\mathcal{E}}_j) C_j (\mathcal{E}(u) - \bar{\mathcal{E}}_j). \quad (3)$$

In (3), Hooke's law is assumed and

$$\mathcal{E} = \mathcal{E}(u) = \mathcal{E}_{ij}(u) := \frac{1}{2} (\partial_i u_j + \partial_j u_i)$$

is the (linearised) strain tensor,  $\bar{\mathcal{E}}_j$  the eigenstrain of phase  $j$ .  $C$  is the elasticity tensor that maps symmetric tensors in  $\mathbb{R}^{D \times D}$  onto itself. We assume that  $C$  is symmetric, positive definite and does not depend on  $\varrho$  and  $\chi$ . The existence result below holds more generally even for  $C = C(\varrho)$ , but this case cannot be treated by our numerical solution method. Finally,  $S := \partial_\varepsilon W^{el}(\chi, \mathcal{E}(u))$  denotes the stress tensor with  $W^{el} := \chi W_1^{el} + (1 - \chi)W_2^{el}$ .

The free energy of the system is defined by

$$\begin{aligned} F(\varrho(t), \chi(t), u(t)) &= \int_{\Omega} f(\varrho(t), \chi(t), u(t)) = \sigma \int_{\Omega} |\nabla \chi(x, t)| dx + F^{out}(u(t)) \\ &+ \int_{\Omega} \chi(t) f_1(\varrho(t), u(t)) + (1 - \chi(t)) f_2(\varrho(t), u(t)) dx \end{aligned} \quad (4)$$

where the first term defines the interfacial surface energy with the (constant) surface tension  $\sigma > 0$ . The term  $F^{out}(u) := \int_{\Omega} \bar{W}(\mathcal{E}(u))$  represents energy effects due to applied outer forces with dead loads.

To summarize, for a given stop time  $T_0 > 0$  we want to study the system:

*Find for  $t \geq 0$  a vector  $(\varrho, \chi, \mu, u)$  such that in  $\Omega_{T_0} := \Omega \times (0, T_0)$*

$$\partial_t \varrho = \operatorname{div}(L \nabla \mu), \quad (5)$$

$$\mu = \frac{\partial f}{\partial \varrho}(\varrho, \chi, u), \quad (6)$$

$$\operatorname{div}(S) = 0, \quad (7)$$

$$S = \partial_\varepsilon W^{el}(\chi, \mathcal{E}(u)), \quad (8)$$

$$F(\varrho(t), \chi(t), u(t)) = \min_{\tilde{\chi} \in X} F(\varrho(t), \tilde{\chi}, u(t)) \quad (9)$$

with the initial data for  $t = 0$  in  $\Omega$

$$\varrho(\cdot, 0) = \varrho_0(\cdot) \quad (10)$$

and boundary conditions for  $t > 0$  in  $\partial\Omega$

$$\varrho = \varrho_d, \quad L \nabla \mu \cdot \vec{\nu} = 0, \quad S \vec{\nu} = \bar{S} \vec{\nu}. \quad (11)$$

## Remarks:

- Simple examples show that the solutions of (5)–(11) are in general not unique because of a possible non-uniqueness of  $\chi$ .
- Equation (9) does not control the variation of  $\chi$  in time.
- Equations (7), (9) state that the deformations resp. the phase parameter adapt infinitely fast to diffusion.
- The existence of a minimum in Equation (9) w.r.t.  $\chi$  is guaranteed by the Poincaré inequality and the term  $\sigma|\nabla\chi|$  in the definition of  $F$ .

The following existence result is shown in [4] under mild assumptions on  $f_j$  that in particular are fulfilled for the choices (1) and (2). It is formulated for  $\varrho_D = 0$ .

**Theorem 1:** *(Global existence for the sharp interface model)*

*There exists a weak solution  $(\varrho, \mu, \chi, u)$  of the sharp interface equations (5)–(11) with logarithmic or polynomial free energy such that*

- (i)  $\varrho \in C^{0, \frac{1}{4}}([0, T_0]; L^2(\Omega; \mathbb{R}^n))$ ,
- (ii)  $\partial_t \varrho \in L^2(0, T_0; (H_0^1(\Omega; \mathbb{R}^n))')$ ,
- (iii)  $\chi \in L^1(0, T_0; BV(\Omega))$ ,
- (iv)  $u \in L^\infty(0, T_0; H^1(\Omega, \mathbb{R}^D))$ ,
- (v)  $\mu \in L^2(0, T_0; H^1(\Omega, \mathbb{R}^n))$ ,
- (vi)  $\ln \varrho_j \in L^1(\Omega_{T_0})$  for  $1 \leq j \leq n$  and in particular  $0 < \varrho_j < 1$  a.e.

Theorem 1 states for space dimensions  $D \leq 2$  as a consequence of Sobolev's embedding theorem that  $\mu$  is a continuous function. This implies a jump condition on  $\varrho$  across the interface as we shall see.

## 3 Numerical solution method

The numerical implementation is based on linear finite elements. The algorithm will be implemented for  $\Omega \subset \mathbb{R}^2$ . It is assumed that  $\partial\Omega$  is polygonally bounded in order to avoid problems with the approximation of the boundary. By  $\mathcal{T}^h$  we denote a triangulation of  $\Omega$  where  $h$  refers to the maximum

distance of two neighbouring vertices. In two space dimensions we assume that  $\mathcal{T}^h$  is weakly acute, see [7], this means that the sum of opposite angles relative to any side does not exceed  $\pi$ . The vertices of the triangulation are denoted by  $\{x_j\}_{1 \leq j \leq N^h}$  for  $N^h \in \mathbb{N}$ . The linear basis functions associated with  $\mathcal{T}^h$  are denoted by  $\varphi_i$ ,  $1 \leq i \leq N^h$ . They are uniquely determined by the condition  $\varphi_i(x_j) = \delta_{ij}$ , where  $\delta_{ij}$  is the Kronecker symbol. The space of linear finite elements is denoted by

$$S^h := \left\{ \varphi \in C^0(\bar{\Omega}) \mid \varphi|_T \text{ is linear for all } T \in \mathcal{T}^h \right\} \subset H^{1,2}(\Omega).$$

One can think up several algorithms to solve System (5)-(11). The direct approach is a standard discretisation of Equation (5) by using an implicit Euler scheme (or some other stable time discretisation), determining  $\varrho$  immediately from Equation (5). But as numerical tests have revealed, this method is not very efficient and has several shortcomings. As  $\varrho$  jumps across an interface, two numerical grids (one for each phase) are needed and the computation of  $\varrho$  becomes complicated and slow.

The algorithm we want to propose makes use of the fact that the potential  $\mu$  is a continuous function and does not jump across a transition layer. We will formulate an evolution equation for  $\mu$  that is iterated against the other equations. Thus, when solving the equation for  $\mu$ , see (15) below,  $\chi$  is given from the previous iteration step and due to the convexity of  $f_l$  in  $\varrho$  one can reconstruct  $\varrho$  from  $\mu$ .

To make this precise, let  $f_l$  be defined by (1). We find

$$\mu_i(\varrho, \chi) = (\chi \hat{\varrho}_1 + (1 - \chi) \hat{\varrho}_2) \varrho_i - (\chi \bar{\varrho}_{i1} + (1 - \chi) \bar{\varrho}_{i2})$$

and therefore

$$\varrho_i(\mu, \chi) = \frac{\mu_i + \chi \bar{\varrho}_{i1} + (1 - \chi) \bar{\varrho}_{i2}}{\chi \hat{\varrho}_1 + (1 - \chi) \hat{\varrho}_2}. \quad (12)$$

Similarly, if  $f$  is given by (2),

$$\mu_i(\varrho, \chi) = (\chi \alpha_1 + (1 - \chi) \alpha_2) (\ln \varrho_i + 1) =: \alpha_\chi (\ln \varrho_i + 1)$$

and hence

$$\varrho_i(\mu) = \exp \left( \frac{\mu_i - \alpha_\chi}{\alpha_\chi} \right). \quad (13)$$

The jump condition for  $\varrho$  across an interface is found from the condition  $\mu(\varrho, \chi = 0) = \mu(\varrho, \chi = 1)$ . For  $f_l$  defined by (1) this condition reads

$$\hat{\varrho}_{i2}(\varrho_i|\{\chi = 0\} - \bar{\varrho}_{i2}) = \hat{\varrho}_{i1}(\varrho_i|\{\chi = 1\} - \bar{\varrho}_{i1}), \quad 1 \leq i \leq n. \quad (14)$$

After this general introduction to the algorithm we will now describe the details. For time step  $m \in \mathbb{N}_{>0}$ , let  $\varrho^{m,0} := \varrho^{m-1}$  and  $\chi^{m,0} := \chi^{m-1}$ , where  $(\varrho^{m-1}, \chi^{m-1})$  is the solution pair of time step  $m-1$  (if  $m=1$ , an initial minimisation step solving (9) is carried out to compute  $\chi^{1,0} = \chi^0$  and  $\varrho^0$  is given by the initial values  $\varrho_0$ ).

For  $k \geq 1$  the algorithm consists of the following five steps:

**Step 1: Computation of  $\mu^{m,k}$**

To fix the computations, let  $f_j$  be defined by (1). Therefore

$$\begin{aligned} \mu_i^{m,k} &= \sum_{j=1}^2 \chi_j^{m,k} \hat{\varrho}_{ij}(\varrho_i^{m,k} - \bar{\varrho}_{ij}), \\ \mu_i^{m-1} &= \sum_{j=1}^2 \chi_j^{m-1} \hat{\varrho}_{ij}(\varrho_i^{m-1} - \bar{\varrho}_{ij}) \end{aligned}$$

which yields directly for any  $i \in \{1, \dots, n\}$

$$\begin{aligned} \mu_i^{m,k} - \mu_i^{m-1} &= \sum_{j=1}^2 \left\{ \chi_j^{m,k} \hat{\varrho}_{ij}(\varrho_i^{m,k} - \varrho_i^{m-1}) + (\chi_j^{m,k} - \chi_j^{m-1}) \hat{\varrho}_{ij}(\varrho_i^{m-1} - \bar{\varrho}_{ij}) \right\} \\ &\approx \sum_{j=1}^2 \hat{\varrho}_{ij} \left\{ \chi_j^{m,k-1} (\tau \operatorname{div}((L \nabla \mu^{m,k})_i)) + (\chi_j^{m,k-1} - \chi_j^{m-1})(\varrho_i^{m-1} - \bar{\varrho}_{ij}) \right\}. \end{aligned} \quad (15)$$

In the last line,  $\chi_j^{m,k}$  has been replaced by  $\chi_j^{m,k-1}$  which is the heart of a predictor-corrector method.  $\tau > 0$  denotes the step size of the finite difference quotient to resolve  $\partial_t \varrho$  (implicit Euler scheme). Let

$$\Omega_j := \left\{ x \in \Omega \mid \chi_j^{m,k-1}(x) = 1 \right\} \quad \text{for } j = 1, 2$$

and

$$\cup_l \Gamma_{jl} = \partial \Omega_j \setminus \partial \Omega.$$

For the solution of (15) one integrates over  $\Omega$  and tests with  $\varphi_\beta$ ,  $1 \leq \beta \leq N^h$ . In order to calculate the first term of the right hand side in (15) we compute with the help of the divergence theorem for any  $i \in \{1, \dots, n\}$

$$\begin{aligned}
\int_{\Omega} \sum_{j=1}^2 \chi_j^{m,k-1} \hat{\varrho}_{ij} \operatorname{div}((L\nabla\mu^{m,k})_i) \varphi_{\beta} &= \sum_{j=1}^2 \hat{\varrho}_{ij} \int_{\Omega_j} \operatorname{div}((L\nabla\mu^{m,k})_i) \varphi_{\beta} \\
&= \sum_{j=1}^2 \hat{\varrho}_{ij} \left( \int_{\partial\Omega_j} (L\nabla\mu^{m,k})_i \cdot \vec{\nu} \varphi_{\beta} - \int_{\Omega_j} (L\nabla\mu^{m,k})_i \cdot \nabla \varphi_{\beta} \right) \\
&= \sum_{j=1}^2 \hat{\varrho}_{ij} \left( \sum_l \int_{\Gamma_{jl}} (L\partial_{\nu} \mu^{m,k})_i \varphi_{\beta} - \int_{\Omega_j} (L\nabla\mu^{m,k})_i \cdot \nabla \varphi_{\beta} \right) \\
&= \sum_{j=1}^2 \hat{\varrho}_{ij} \left( \sum_l \int_{\Gamma_{jl}} \sum_{r=1}^n L_{ir} \sum_{\alpha=1}^{N^h} v_{r,\alpha}^{m,k} \partial_{\nu} \varphi_{\alpha} \varphi_{\beta} \right. \\
&\quad \left. - \int_{\Omega_j} \sum_{r=1}^n L_{ir} \sum_{\alpha=1}^{N^h} v_{r,\alpha}^{m,k} \nabla \varphi_{\alpha} \cdot \nabla \varphi_{\beta} \right) \\
&=: \sum_{j=1}^2 \hat{\varrho}_{ij} M^j v_i^{m,k},
\end{aligned}$$

where the matrices  $M^j = M^j(\chi^{m,k-1}, \mu^{m,k}) \in \mathbb{R}^{N^h} \times \mathbb{R}^{N^h}$  are defined by the last identity and the relationship  $\mu_i^{m,k} = \sum_{\alpha=1}^{N^h} v_{i,\alpha}^{m,k} \varphi_{\alpha}$  is assumed with  $v_i^{m,k} = (v_{i,1}^{m,k}, \dots, v_{i,N^h}^{m,k}) \in \mathbb{R}^{N^h}$ .

The solution of (15) in matrix form to determine the approximate solution in the finite element space  $S^h$  is straightforward and the details are left out.

### Step 2: Computation of $\varrho^{m,k}$

This is done as described in the beginning of this section and  $\varrho^{m,k}$  is computed by (12) resp. (13).

### Step 3: Computation of $u^{m,k}$

The deformation  $u^{m,k}$  is obtained by solving the weak formulation of the elliptic equation

$$\operatorname{div}(\partial_{\mathcal{E}} W^{\text{el}}(u^{m,k}, \chi^{m,k-1})) = 0 \quad \text{in } \Omega.$$

**Step 4: Computation of  $\chi^{m,k}$** 

This is the most difficult part of the algorithm. From Step 2 and Step 3,  $\varrho^{m,k}$ ,  $u^{m,k}$  are known for the minimisation process of Equation (9). The complete algorithm to approximately compute the global minimiser is presented in the subsequent section.

**Step 5: Iteration**

Iterate in  $k$  by restarting with Step 1 until the difference  $\|\varrho^{m,k} - \varrho^{m,k-1}\|_{L^2}$  and  $\|\chi^{m,k} - \chi^{m,k-1}\|_{BV}$  is small.

If  $\varrho \mapsto f_l(\varrho, u) \in C^{1,1}((\mathbb{R}^+)^n)$  and  $u \mapsto f_l(\varrho, u) \in C^{0,1}(\mathbb{R}^D)$ , Banach's fixed point theorem guarantees for sufficiently small  $\tau > 0$  the convergence of the iteration scheme.

## 4 The minimisation algorithm for $\chi$

We introduce a general method to compute the minimum in (9). The algorithm will not find a global minimizer in all cases, but the exceptions can be classified. We will start with a description of the basic version, then discuss the improvement.

**Basic Algorithm**

At  $t = 0$  we generate a start front. We initialize with  $\chi \equiv 1$  in  $\Omega$ . We loop over all  $T \in \mathcal{T}^h$  and set  $\chi(x_j) := 0$  for all vertices  $x_j \in T$  if

$$\min_{x \in T} (f_1 - f_2)(\varrho(x), u(x)) > \sigma(|\partial T| - |\partial T \cap \partial \Omega|).$$

Then we set

$$\Gamma_{\text{start}} := \overline{\partial\{x \in \Omega \mid \chi(x) = 0\}} \cap \overline{\partial\{x \in \Omega \mid \chi(x) = 1\}} \cap \Omega.$$

In this way, some fronts are not detected which is no problem as the extension discussed below will find them. This strategy makes sure that  $\Gamma_{\text{start}}$  does not contain parts which should be removed to lower  $F$ .

To optimize the position of  $\Gamma_{\text{start}}$  we use a front propagation similar to the fast marching method. This basic algorithm only finds local minimisers.

On  $\Gamma$  we choose once and for all one of the two normal directions and introduce the level set function  $\psi$  by

$$\psi(x, t) := \begin{cases} +\text{dist}(x, \Gamma(t)), & \text{if } \chi(x, t) = 0, \\ -\text{dist}(x, \Gamma(t)), & \text{if } \chi(x, t) = 1. \end{cases}$$

This definition implies

$$\Gamma(t) = \{x \in \Omega \mid \psi(x, t) = 0\}.$$

The program uses  $\psi$  instead of  $\chi$  as variable.

The variation of  $\psi$  in time in normal direction depending on a variation  $\zeta$  is formalised by the level set equation

$$\partial_s \psi = \|\nabla \psi\| \zeta. \quad (16)$$

Here,  $\|\cdot\|$  denotes the Euklidian norm in  $\mathbb{R}^2$  and we write  $s$  instead of  $t$  to emphasize that we introduced an artificial time variable which is different from the one in Equation (5) resp. Equation (15).

We use Equation (16) to propagate the front  $\Gamma$ . Possible directions in (16) are spanned by the basis functions  $\varphi_i \in S^h$ ,  $1 \leq i \leq N^h$ . We construct a gradient flow in directions of steepest descent of  $F$  using the representation

$$\nabla_{\psi} F(\psi_0) := \left( \frac{\partial F}{\partial \varphi_1}(\psi_0), \dots, \frac{\partial F}{\partial \varphi_{N^h}}(\psi_0) \right). \quad (17)$$

Here,  $\psi_0$  denotes for the first run of Equation (16) in time step  $l$ , i.e.  $t = l\tau$ , the level set function corresponding to  $\Gamma((l-1)\tau)$ . The computation of  $\frac{\partial F}{\partial \varphi_i}(\psi_0)$  is explained below.

In (16) we choose

$$\zeta := \sum_{i=1}^{N^h} \alpha_i \varphi_i$$

together with the setting

$$\alpha_i := \bar{\alpha} \left( -\text{sgn} \frac{\partial F}{\partial \varphi_i}(\psi_0) \right)_+ \|\nabla_{\psi} F(\psi_0)\|. \quad (18)$$

In (18),  $(g)_+$  denotes the positive part of a function  $g$  which guarantees that only descent directions of  $F$  are selected, and  $\bar{\alpha} > 0$  is an arbitrary constant

that determines the speed by which the algorithm propagates the front in every iteration step w.r.t.  $s$ . For each time step  $t = \tau l$  of Equation (15) we pass to the limit  $s \rightarrow \infty$  in (16), i.e. we step through an inner loop until

$$\|\nabla_\psi F(\psi_0)\| < \varepsilon_0$$

for a given small  $\varepsilon_0 > 0$ .

Summing up, we obtain a method that decreases the free energy  $F$  by moving  $\Gamma$  in a way that mimics the steady movement of a front in nature.

We still have to explain how for given  $\psi$  the partial derivatives of  $F$  are obtained from (17). An application of the chain rule yields:

$$\begin{aligned} \frac{\partial F}{\partial \varphi_i}(\psi_0) &= \lim_{s \rightarrow 0} \frac{F(\psi_0 + s\|\nabla\psi_0\|\varphi_i) - F(\psi_0)}{s} \\ &= DF(\psi_0) \|\nabla\psi_0\|\varphi_i. \end{aligned}$$

These equalities are formal since the argument  $\psi_0 + s\|\nabla\psi_0\|\varphi_i \notin S^h$ . But when splitting the volume integrals we find:

$$\begin{aligned} \frac{\partial F}{\partial \varphi_i}(\psi_0) &= \sum_{T \in \mathcal{T}^h} \frac{d}{ds} \int_T f(\psi_0 + s\|\nabla\psi_0\|\varphi_i) dx \Big|_{s=0} + \frac{\partial F_S}{\partial \varphi_i}(\psi_0) \\ &= \sum_{T \in \mathcal{T}^h} \int_T \frac{\partial f}{\partial \psi}(\psi_0) \|\nabla\psi_0\|\varphi_i dx + \frac{\partial F_S}{\partial \varphi_i}(\psi_0). \end{aligned}$$

Here,  $\frac{\partial F_S}{\partial \varphi_i}(\psi_0)$  corresponds to the integral  $\int_\Omega |\kappa|$ , where  $\kappa$  is the mean curvature of  $\Gamma$ .

### Extension of the Algorithm

The generation of  $\Gamma_{\text{start}}$  and propagation of the front is done as before. Additionally we now set up a refinement mechanism that puts us in the position to detect new fronts that may arise within a bulk phase.

In accordance to the numerical solution scheme we can assume that  $\varrho$  and  $u$  are given functions.

Let us fix a vertex  $x_j$  of the triangulation  $\mathcal{T}^h$  and let

$$\omega_{x_j} := \text{supp } \varphi_j = \overline{\{x \in \Omega \mid \varphi_j(x) \neq 0\}},$$

where  $\varphi_j$  is the linear basis function corresponding to  $x_j$ , see Figure 1. By  $\text{tr}(\gamma)$  we denote the trace of a closed curve  $\gamma$  and by  $\text{Int}(\gamma)$  its interior, that is the domain enclosed by  $\gamma$ .

As we want to detect new fronts within the bulk phase we assume  $\chi \equiv 0$  in  $\omega_{x_j}$  initially. The other case  $\chi \equiv 1$  in  $\omega_{x_j}$  is treated analogously.

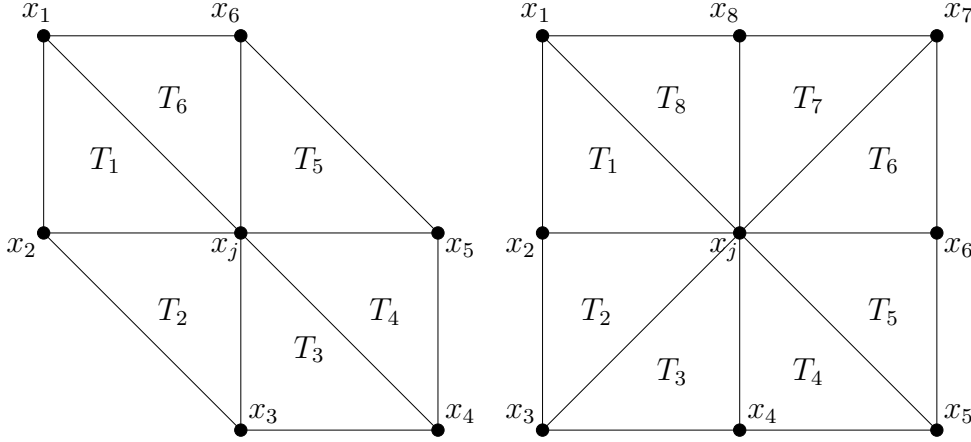


Figure 1: Two examples for  $\omega_{x_j}$ , vertex  $x_j$  and adjacent triangles

In order to accurately solve (9) we ask under which conditions there exists a closed curve  $\gamma$  around  $x_j$  with  $\text{tr}(\gamma) \subset \omega_{x_j}$  such that  $\chi \equiv 1$  in  $\text{Int}(\gamma)$  and  $\chi \equiv 0$  in  $\omega_{x_j} \setminus \text{Int}(\gamma)$ . If  $\omega_{x_j}$  contains such an interface  $\gamma$ , the free energy restricted to  $\omega_{x_j}$  is

$$F(\varrho, \chi, u)|_{\omega_{x_j}} = \sigma \int_{\omega_{x_j}} |\nabla \gamma| + \int_{\text{Int}(\gamma)} f_1(\varrho, u) + \int_{\omega_{x_j} \setminus \text{Int}(\gamma)} f_2(\varrho, u).$$

As initially  $\chi \equiv 0$  in  $\omega_{x_j}$ , the solution with interface is energetically favorable if

$$\int_{\omega_{x_j}} f_2(\varrho, u) > \int_{\text{Int}(\gamma)} f_1(\varrho, u) + \int_{\omega_{x_j} \setminus \text{Int}(\gamma)} f_2(\varrho, u) + \sigma \int_{\omega_{x_j}} |\nabla \gamma|$$

or equivalently

$$\int_{\text{Int}(\gamma)} (f_2(\varrho, u) - f_1(\varrho, u)) > \sigma \int_{\omega_{x_j}} |\nabla \gamma|. \quad (19)$$

If  $V := |\int_{\text{Int}(\gamma)} dx|$  denotes the area enclosed by the interface  $\gamma$  and  $L := \int_{\omega_{x_j}} |\nabla\gamma|$  its perimeter (length of  $\gamma$ ), the *Isoperimetric Inequality* in two space dimensions states that

$$L^2 \geq 4\pi V \quad (20)$$

with equality only if  $\gamma$  is a circle with perimeter  $L$ .

With the help of the isoperimetric inequality we immediately find

$$\sigma \int_{\omega_{x_j}} |\nabla\gamma| \geq \sigma \sqrt{4\pi |\text{Int}(\gamma)|}$$

and consequently there is certainly **no** front  $\gamma$  contained in  $\omega_{x_j}$  if

$$\sigma \sqrt{4\pi |\text{Int}(\gamma)|} \geq \int_{\text{Int}(\gamma)} (f_2(\varrho, u) - f_1(\varrho, u)).$$

We define constants

$$\begin{aligned} M_0 &:= \min\{(f_2 - f_1)(\varrho(x_i), u(x_i)) \mid x_i \text{ vertex in } \omega_{x_j}\}, \\ M_1 &:= \min\{(f_1 - f_2)(\varrho(x_i), u(x_i)) \mid x_i \text{ vertex in } \omega_{x_j}\}. \end{aligned}$$

Since

$$\int_{\text{Int}(\gamma)} (f_2(\varrho, u) - f_1(\varrho, u)) \geq M_0 V,$$

the condition  $\sigma \sqrt{4\pi} \geq M_0 \sqrt{V}$  affirms that there is no transition layer  $\gamma$  within  $\omega_{x_j}$  enclosing a volume  $V$ . As  $V$  is a priori unknown in this estimate, the formula is replaced by the sufficient condition

$$\sigma \sqrt{4\pi} \geq M_0 \sqrt{|\omega_{x_j}|}. \quad (21)$$

Similarly, if initially  $\chi \equiv 1$  in  $\omega_{x_j}$ , the condition analogous to (21) which ensures that there is **no** front within  $\omega_{x_j}$  is

$$\sigma \sqrt{4\pi} \geq M_1 \sqrt{|\omega_{x_j}|}. \quad (22)$$

The gist of the improvement is now the following refinement strategy. We refine the triangles in  $\omega_{x_j}$  if the following two conditions simultaneously hold:

- $\chi \equiv 0$  in  $\omega_{x_j}$  or  $\chi \equiv 1$  in  $\omega_{x_j}$ .
- Inequality (21) does not hold (if  $\chi \equiv 0$ ) or Inequality (22) does not hold (if  $\chi \equiv 1$ ).

The algorithm works in the following way. It is clear that (21) and (22) are satisfied if  $|\omega_{x_j}|$  is sufficiently small. From the boundedness of  $\varrho$  in  $\Omega_{T_0}$  we infer that there is for all  $\omega_{x_j}$  a maximal number  $n_{\text{ref}}$  of refinements after which these inequalities will be satisfied. Starting from  $\omega_{x_j}$  (refinement step 0), it can be revealed by Condition (19) whether the free energy is diminished by introducing a new front. If not, all triangles in  $\omega_{x_j}$  are refined unless (21) (if  $\chi \equiv 0$  in  $\omega_{x_j}$ ) resp. (22) (if  $\chi \equiv 1$  in  $\omega_{x_j}$ ) are satisfied (maximal refinement step  $n_{\text{ref}}$ ). This guarantees that fronts within  $\omega_{x_j}$  are detected. New fronts connect centres of edges of  $T_i$  and/or corners of  $T_i$  by straight lines. Among all such closed curves the one is taken as new front that yields the smallest free energy.

## Remarks

- The constant  $\sqrt{4\pi}$  that enters the estimates due to the isoperimetric inequality is not optimal for the case considered here as only polygonal interfaces may be generated by the algorithm and the circle is prohibited. Angle conditions on the geometry of the triangles as a consequence of the acuteness of  $\mathcal{T}^h$  influence this constant.
- The maximal number  $n_{\text{ref}}$  of refinement steps may get very large for small  $\sigma$ . For practical reasons it may become necessary to bound  $n_{\text{ref}}$  in order to limit the needed computer memory.
- If after  $n_{\text{ref}}$  local refinement steps of  $\omega_{x_j}$  it is found that no front  $\gamma$  is contained, the original triangulation is restored. This backtracking is essential to avoid waste triangles and keep the numerical effort small. Table 1 below illustrates what happens without this strategy.
- The global optimum in (9) does not depend on the triangulation. But small shifts of  $\mathcal{T}^h$  in direction of a vector  $d$  with  $\|d\| \leq h/2$  may lead to different transition layers. Similarly, the generated closed fronts around a vertex  $x_j$  are piecewise linear, even though the shape of the curve is not exactly known. This explains why the numerical

scheme usually does not find the optimal solution, but the computed  $\chi$  minimizes  $F$  up to an error of order  $O(h)$ .

- The presented algorithm generates closed interfaces around a vertex  $x_j$  where  $(f_2 - f_1)(\varrho, u)$  is small (if  $\chi \equiv 0$  in a neighbourhood) or where  $(f_1 - f_2)(\varrho, u)$  is small (if  $\chi \equiv 1$  in a neighbourhood). Hence, it operates similar to Heuygen's principle in fluid dynamics. For the generation of fronts it is essential that if a new curve  $\gamma$  inside a triangle  $T_l$  is about to be added and if  $T_l$  already contains an interface (in particular due to the creation of a circular front around a neighbouring vertex), the new and the old interface are merged to one transition layer if this leads to an energy reduction. In this way, by stepping over all vertices, a unique front can form, see Figure 2.

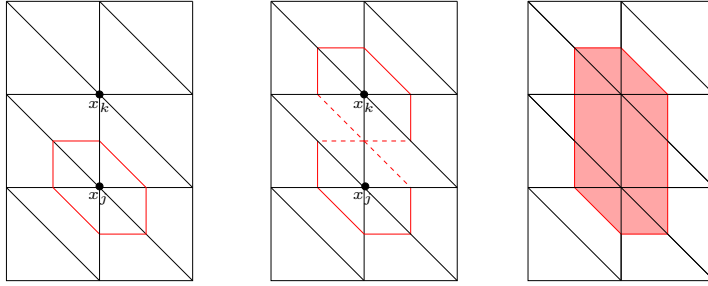


Figure 2: Joining of two closed curves to one front

- There are two relevant cases adjacent to the boundary where  $\partial\Omega$  shortens the interface and  $\gamma$  is no longer a closed curve. For simplicity we assume that  $\Omega$  is a rectangular domain and that  $\omega_{x_j} \cap \partial\Omega$  is simply connected. The first situation ( $k = 1$ ) is that  $\omega_{x_j}$  is close to a corner. For the isoperimetric inequality, the optimal shape is now a segment of the circle with a  $90^\circ$  angle. The second situation ( $k = 2$ ) is that  $\omega_{x_j}$  is close to a straight boundary and the optimal contour is a half-circle. In either case, (20) must be changed to  $L^2 \geq k\pi V$  and Conditions (21),(22) read now  $\sigma\sqrt{k\pi} \geq M_{0/1}\sqrt{|\omega_{x_j}|}$ .
- With the extension, the algorithm even masters the splitting of one phase into two smaller ones. Yet, the conditions (19), (21) and (22) are local and may lead to wrong results. In this regard one must take particular care of the start triangulation. The difficulties that

go along with the detection of the transition layer at  $t = 0$  and the non-coarseness of the grid are illustrated by Figure 3.

In the setting of Figure 3, the domain  $\Omega$  is a long and thin pipe with height  $H > 0$ . In the left part  $\Omega_A$  the density fulfils  $\varrho \equiv \varrho_A$ , and  $\varrho \equiv \varrho_B$  in  $\Omega_B$ . We assume  $|\Omega_A| = |\Omega_B| = |\Omega|/2$  and  $\chi \equiv 0$  initially. Let  $\delta := f_2(\varrho_A) - f_1(\varrho_A) > 0$  be small.

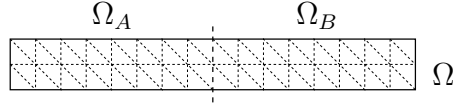


Figure 3: Exceptional case where the interface (dashed line) is not found

The flipping over from  $\chi \equiv 0$  in  $\Omega_A$  to  $\chi \equiv 1$  in  $\Omega_A$  is energetically favorable if

$$\Delta F = -\delta|\Omega_A| + \sigma H < 0.$$

The free energy difference  $\Delta F$  of the two configurations is presumed negative because  $|\Omega_A|$  is large and  $H$  small (choose constants accordingly). Therefore, the optimal  $\chi$  to Figure 3 corresponds to two phases separated by a transition layer along the dashed line in the middle.

First we analyse the behaviour of the basic algorithm as  $\Gamma_{\text{start}}$  is generated. Let  $T \subset \Omega_A$  be a triangle adjacent to the dashed line. There is **no** flipping over from  $\chi \equiv 0$  in  $\Omega_A$  to  $\chi \equiv 1$  in  $T$  if

$$\Delta F_{|T} = -\delta|T| + \sigma(|\partial T| - |\partial T \cap \partial \Omega|) > 0. \quad (23)$$

This inequality can hold as  $\delta$  is small and  $|T|$  is small. (This is also clear by regarding the dimension:  $|T|$  scales with  $h^2$ ,  $|\partial T|$  with  $h$ . Thus, if  $h$  is small enough initially, (23) is satisfied.)

Therefore, any triangle-based algorithm to generate  $\Gamma_{\text{start}}$  that exploits only local information will fail. The same difficulty causes also the failure of the extended algorithm: If  $x_j \in \Omega_A$  is a vertex and if we flip in  $\omega_{x_j}$  from  $\chi \equiv 0$  to  $\chi \equiv 1$ , the gain in bulk energy is  $|\omega_{x_j}|\delta \sim h^2$ , but  $F$  is increased by  $F_S := |\partial \omega_{x_j}| \sim h$ . Again for  $h$  small enough, no new front around  $x_j$  is added. This is also true for  $x_j \in \overline{\Omega_A} \cap \partial \Omega$ .

To conclude, we see that no transition layer separating  $\Omega_A$  and  $\Omega_B$  is added in the situation of Figure 3 by the algorithm as would be

correct. Instead, the whole of  $\Omega$  is treated as one phase. The reason is that the decrease in volume energy does not compensate the increase in surface energy. This is because the start triangulation is too fine and the algorithm exploits only local information.

- There are examples of initial values where the evolution of  $\chi$  for  $t > 0$  is unclear. The typical setting is a junction of two phases in a chess-board pattern touching in one point at  $t = 0$ , see the first picture in Figure 4. At  $t > 0$  either the black phase is simply connected (right picture) or the white phase (picture in the centre). In nature this is determined by properties on the microscale not inherent in the model. In the numerical algorithm the ordering of the finite elements determines which of the two solutions is found. The case presented in Figure 4 is thoroughly discussed in [5] for the Allen-Cahn equation.

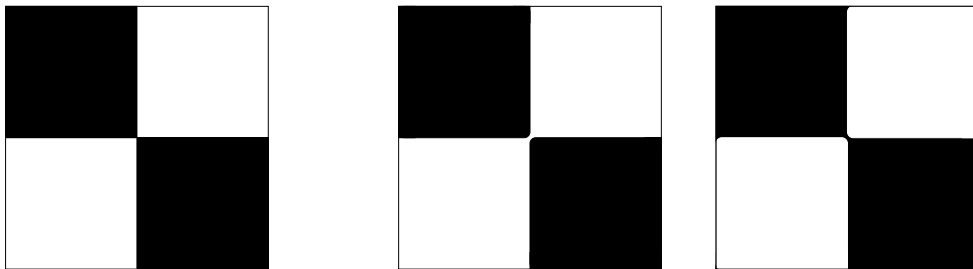


Figure 4: Initial condition and two possible configurations for  $t > 0$

## 5 A stationary solution

For this and the following section we let  $F^{\text{out}} \equiv 0$ . We will compute a stationary solution of (5)-(11) used to test the algorithm. We neglect elasticity,  $W^{\text{el}} \equiv 0$ , assume  $\Omega = B_1(0) \subset \mathbb{R}^2$ ,  $n = 1$ , and set  $f_j(\varrho) = \frac{\hat{\varrho}_j}{2}(\varrho - \bar{\varrho}_j)^2$ . We are going to construct rotationally symmetric functions  $\varrho = \varrho(r)$  and  $\chi = \chi(r)$ , where  $(r, \varphi)$  are the polar coordinates in  $\mathbb{R}^2 \setminus \{0\}$ .

For a given radius  $0 < r_0 < 1$  we postulate the stationary solution

$$\varrho(x) = \begin{cases} \varrho_A & \text{for } |x| < r_0, \\ \varrho_B & \text{for } |x| > r_0 \end{cases}, \quad \chi(x) = \begin{cases} 1 & \text{for } |x| < r_0, \\ 0 & \text{for } |x| > r_0 \end{cases} \quad (24)$$

where  $\varrho_A, \varrho_B$  are positive real constants to be determined later.

Let us compare the free energy  $F_0$  of the start configuration with the free energy  $F_1$  where the jump is located at a smaller radius  $0 < r_1 < r_0$ ,

$$\chi(x) = \begin{cases} 1 & \text{for } |x| < r_1, \\ 0 & \text{for } |x| > r_1 \end{cases} \quad (25)$$

and with the free energy  $F_2$  where the jump is positioned at a larger radius  $r_0 < r_2 < 1$ , and  $\chi$  is given as in (25) with  $r_1$  being replaced by  $r_2$ . This reflects the minimisation process with respect to  $\chi$  for fixed  $\varrho$  as we assume that the parameters  $\varrho_A, \varrho_B, \mathcal{T}^h, \sigma, f_l$  are such that no new fronts may arise.

We show now  $F_1 > F_0$  and  $F_2 > F_0$ . We compute

$$\begin{aligned} F_0 &= 2\pi\sigma r_0 + 2\pi r_0 f_1(\varrho_A) + 2\pi(1 - r_0)f_2(\varrho_B), \\ F_1 &= 2\pi\sigma r_1 + 2\pi r_1 f_1(\varrho_A) + 2\pi(r_0 - r_1)f_2(\varrho_A) + 2\pi(1 - r_0)f_2(\varrho_B), \\ F_2 &= 2\pi\sigma r_2 + 2\pi r_0 f_1(\varrho_A) + 2\pi(r_2 - r_0)f_1(\varrho_B) + 2\pi(1 - r_2)f_2(\varrho_B). \end{aligned}$$

We see that  $F_1 > F_0$  is equivalent to

$$\sigma > f_2(\varrho_A) - f_1(\varrho_A) \quad (26)$$

and find  $F_2 > F_0$  to be equivalent to

$$\sigma > f_2(\varrho_B) - f_1(\varrho_B). \quad (27)$$

If (26) and (27) hold,  $(\varrho, \chi)$  defined by (24) is a stationary solution because  $\mu$  is identical to a constant, thus  $\partial_t \varrho = 0$ .

## 6 Numerical results

In the sequel we present the results of some numerical computations.

### A: Analytic test case

In continuation of the last section we verify part of the algorithm by testing with the stationary solution just found. We assume

$$f_1(\varrho) := \varrho^2, \quad f_2(\varrho) := (\varrho - 1)^2.$$

By jump condition (14) we have  $\varrho_A = \varrho_B - 1$  and the conditions (26), (27) are both fulfilled if

$$\sigma > -2\varrho_B + 3.$$

For the numerical computations we chose  $r_0 := 0.25$  and  $\varrho_A := 1$ ,  $\varrho_B := 2$ ,  $\sigma := 2$ . For this choice of parameters, (21), (22) hold and no local refinements are generated.

In the test runs we computed  $\varepsilon_\varrho := \|\varrho(\cdot, 0) - \varrho(\cdot, T_0)\|_{L^2}$  for stop time  $T_0 = 100\tau$  and different refinement levels. The upper part of Table 1 shows the results.  $L$  specifies the refinement level,  $NT$  the number of triangles,  $NN$  the number of generated nodes.

Refinement	$L$	$NT$	$NN$	$\varepsilon_\varrho$
regular	8	1024	561	$4.9 \cdot 10^{-4}$
	10	4096	2145	$1.2 \cdot 10^{-4}$
	12	16384	8385	$3.1 \cdot 10^{-5}$
regular	10	4096	2145	$5.6 \cdot 10^{-6}$
waste	10	19240	9741	$5.6 \cdot 10^{-6}$

Table 1: Comparison of numerical and analytic solution

The second part of Table 1 shows the result of a further test. The only change to the previous setting is  $\sigma := 0.04$  such that  $(\varrho, \chi)$  is no longer stationary and the inner phase grows steadily. The solution is computed both with the standard algorithm and with an artificial modification where the local refinements of  $\omega_{x_j}$  are not undone after noticing that no new fronts are contained. This leads to two additional useless local refinement steps within  $B_{r_0}(0)$ . Here, the  $\varepsilon_\varrho$  column displays the error  $\|\varrho^{\text{reg}} - \varrho^{\text{waste}}\|_{L^\infty(\Omega_{T_0})}$ .

## B: Analysis of jump condition

For  $l = 1, 2$  let  $\Omega_l := \{x \in \Omega \mid \chi_l(x) = 1\}$  and  $\mu^l := \partial_\varrho f_l$ . By testing Equation (5) with  $\zeta \in H^1(\Omega; \mathbb{R}^n)$  we find

$$\int_{\Omega} \partial_t \varrho \zeta = \sum_{l=1}^2 \int_{\Omega_l} \operatorname{div}(L \nabla \mu^l) \zeta = \sum_{l=1}^2 \left( \int_{\partial \Omega_l} L \nabla \mu^l \cdot \vec{\nu} \zeta - \int_{\Omega_l} L \nabla \mu^l \cdot \nabla \zeta \right).$$

By choosing  $\zeta \equiv 1$  we obtain due to (11) and  $\Gamma = \partial \overline{\Omega_1} \cap \partial \overline{\Omega_2} \cap \Omega$

$$\int_{\Omega} \partial_t \varrho = \int_{\Gamma} L(\nabla \mu^1 - \nabla \mu^2) \cdot \vec{\nu}_{|\Omega_1}.$$

If in particular  $\partial_t \varrho = 0$ , the sets  $\Omega_l$  do not depend on  $t$  and we find

$$[L \nabla \mu \cdot \vec{\nu}]_{\Gamma} = 0. \tag{28}$$

Figure 5 is a plot of a stationary solution  $\varrho$  close to a straight interface  $\Gamma$ . For this example we chose  $f_1(\varrho) = \varrho^2$  on the right,  $f_2(\varrho) = 2(\varrho - 1)^2$  on the left of the transition layer and  $L \equiv 1$ .

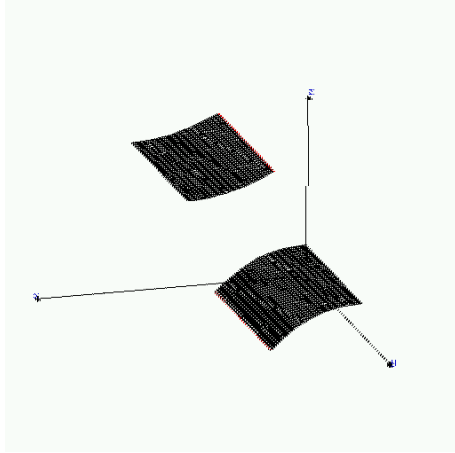


Figure 5: Behaviour of  $\varrho$  close to an interface

From (28), since the normal  $\vec{\nu}$  changes sign, we learn that the graph of  $\varrho$  is bending up on one side of  $\Gamma$  and bending down on the other. The slope of  $\text{graph}(\varrho)$  is larger on the right due to the factor 2 present only in  $f_2$ .

### C: Example of free energy minimisation

In this part we discuss an example which is related to the physical applications and which also illustrates the functioning of the global minimisation in  $\chi$ . Let  $\Omega := (0, 2) \times (0, 1)$ ,  $\varrho = (\varrho_1, \varrho_2)$  and consider

$$f_1(\varrho) := (\varrho_1 - 0.5)^2 + (\varrho_2 - 0.25)^2, \quad f_2(\varrho) := (\varrho_1 - 0.5)^2 + (\varrho_2 - 1)^2.$$

At this example we will study the main mechanism of DIS phenomena as explained in the introduction. We set  $\sigma := 10^{-3}$ ,  $\varrho_{10} \equiv \frac{1}{2}$ ,  $\varrho_{20} \equiv 0$  and solve instead of (5)<sub>2</sub>

$$\partial_t \varrho_2 = \text{div}(L \nabla \mu)_2 + \mathcal{X}_{B_1}$$

where the characteristic function  $\mathcal{X}_{B_1}$  is a source term that leads to an increase of  $\varrho_2$  in  $B_1 := B_{0.25}(0)$ . Thus, during the computation,  $\varrho_2$  grows and at some  $t = t_0$ , in a ball  $B_2$  with radius slightly less 0.25,  $f_2$  becomes preferable which leads to the for DIS phenomena typical flipping over from phase 1 to phase 2 in  $B_2$ .

Due to the source term and the choice of  $\varrho_{01}, \varrho_{02}$ , there is  $\Gamma_{\text{start}} = \emptyset$  and  $\chi(t = 0) \equiv 1$  in  $\Omega$ . At  $t = t_0$ , the new front arising at  $\partial B_2$  is generated by the extended algorithm, and Figure 6 visualizes the main steps. For orientation,  $\partial B_2$  is plotted in green; the fronts generated by the algorithm are plotted in red. First, in succession the triangles within  $B_2$  are refined locally and transition layers around the vertices in  $B_2$  are generated/merged with other fronts (first and second picture). The united interfaces form  $\Gamma \approx \partial B_2$ . The last picture shows the result of the optimisation in  $\chi$  where all superfluous triangulations and hanging nodes have been removed. Only this last picture shows a valid triangulation of  $\Omega$ .

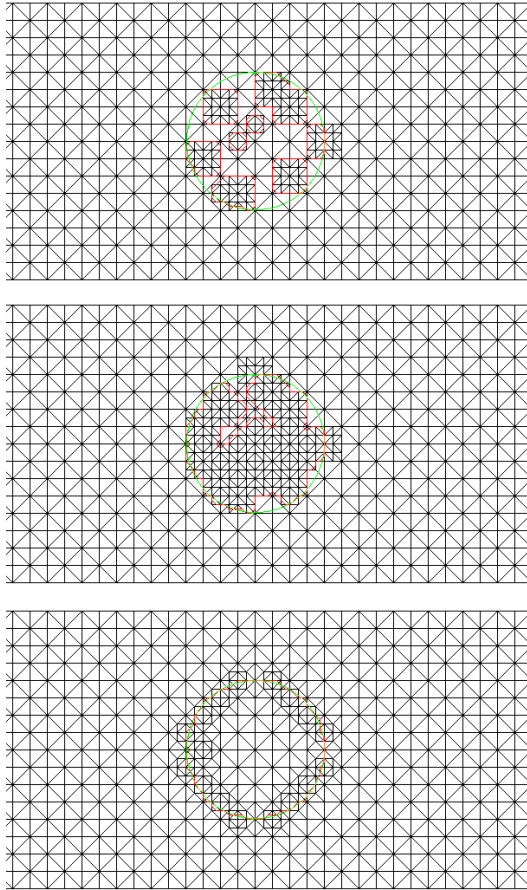


Figure 6: Visualisation of one global minimisation step in  $\chi$

In the later course of the computations, the concentric ball containing phase 2 further grows.

Figure 7 shows  $\varrho_1$  for  $t = t_0 + \tau$ . The jump of  $\chi$  at  $\partial B_2$  leads to a jump of  $\varrho_1$  at  $\partial B_2$ , so the level sets concentrate around the (coarse) approximation of this ball in  $\mathcal{T}^h$ .

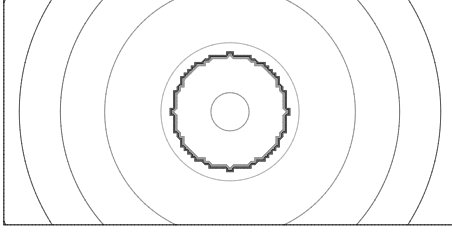


Figure 7: Level sets of  $\varrho_1$  for  $t = t_0 + \tau$

In the physical applications of DIS, the diffuser penetrates the crystal from outside. In the mathematical equations this is modeled by Dirichlet boundary conditions on the diffuser, not by a source term as is done here.

## 7 Discussion

In this article, a mathematical model for DIS was investigated numerically and a computational scheme was presented to approximately find a global minimiser of the free energy. As exemplarily explained at Figure 3, the algorithm does not find the optimal  $\chi$  if  $\mathcal{T}^h$  is too fine. One might think to overcome this problem by reversing the refinement mechanism and considering larger and larger blocks around a vertex  $x_j$ . Our tests have shown that this strategy is in general not practical because  $\mathcal{T}^h$  need not be hierarchical (in contrast to the local refinements of  $\omega_{x_j}$ ) but is usually chosen adaptive to the diffusion of  $\varrho$ . Furthermore, for complex triangulation geometries the numerical effort becomes very large because numerous possible configurations must be tested. Instead, our experience has shown that by a careful analysis before the computations and by choosing a reasonable  $\mathcal{T}^h$  and  $\tau$ , one can ensure that our algorithm finds an optimal  $\chi$ .

The presented algorithm for solving (5)-(11) exploits the continuity of  $\mu$ . Thus the ansatz breaks down in space dimensions  $D \geq 3$ . Also, the method cannot be used if  $W^{el}$  depends on  $\varrho$ , because then one cannot find the analogue of (12) or (13) and recover  $\varrho$  from  $\mu$ . In the other cases, numerical investigations have shown that our method is superior to the standard discretisation where  $\varrho$  is computed directly as the solution to (5).

Looking at the numerical example C, one might try to use the information about the diffusor, here  $\varrho_2$ , to construct or predict the position of new fronts within a bulk phase. Since we also want to use the algorithm in more general settings where the free energies  $f_j$  are not given by an analytic formula but are obtained by ab-initio methods we do not favour this strategy.

## Acknowledgements

The authors thank the German Research Community DFG for the financial support within the priority program 1095 *Analysis, Modeling and Simulation of Multiscale Problems*.

## References

- [1] S. Arnrich, S. Luckhaus, A mathematical model for Phase Transitions in Crystals, Preprint No. 147 (2004), DFG Priority Program 1095 Analysis, Modeling and Simulation of Multiscale Problems
- [2] K. Bente and T. Doering, Eur.J.Miner. **10**(1993), 465
- [3] T. Blesgen, S. Luckhaus and K. Bente, Diffusion induced segregation in the case of the ternary system sphalerite, chalcopyrite and cubanite, submitted to Cryst.Res.Tech.
- [4] T. Blesgen and U. Weikard, A sharp interface model for phase transitions in crystals with linear elasticity, Math. Meth. Appl. Sci. **27**(2004)
- [5] T. Ilmanen, Convergence of the Allen-Cahn Equation to Brakke's motion by Mean Curvature, J. Diff. Geometry **38** (1993), 417–461
- [6] S. Luckhaus, The Stefan problem with the Gibbs-Thomson law, Preprint Universita di Pisa 2.75(591), Pisa (1991)
- [7] R.H. Nochetto, Finite element methods for parabolic free boundary problems, Advances in numerical analysis, **1**(1991), 34–95
- [8] P.I. Plotnikov, V.N. Starovojtov, The Stefan problem with surface tension as the limit of the phase field model, J. Diff. Eq. **29**(1993), 395–404
- [9] W. Ziemer, Weakly differentiable functions, Springer New York (1989)